

SUPPORTING INFORMATION

Exfoliation methods

Two different techniques (sonication and ball milling) were used to prepare the samples, with two different conditions each (high and low power, see table S2). Fig. 2 in main text shows SEM images of the starting BN powder and of the typical solutions obtained.

For sonication test, suspensions were prepared at same starting concentration (3 mg/ml) in IPA and sonicated at different times (20, 40, 60 and 80 hours) using an Elmasonic P70 Ultrasonic Bath at 220W or 66W of effective power.

A planetary ball mill (Retsch PM100) with a 50 ml Zirconium dioxide grinding jar and ≈ 1300 zirconium oxide balls (3 mm in diameter) was used to mill BN powders in IPA at different times (from 1 to 60 hours) and rotation speeds (200 and 450 rpm). After the exfoliation, a centrifuge Heraeus (Omnifuge 2 RS) was used to remove the larger, mesoscopic BN particles.

Upon exfoliation, BN solutions show a whitish colour and a strong light scattering (Fig. 2c), due to the presence of the BN sheets. At difference with graphene, that is exfoliated using high boiling solvents, we exfoliated BN using as solvent isopropanol (IPA) which is a low boiling point solvent (b.p.=82 °C), quick to volatilize and easy to remove after BN processing on surfaces or in composites, thus minimizing processes of flake aggregation. Exfoliation in IPA yields stable solutions of BN.

Both in ball milling and sonication mechanical forces act on the material; however, these forces have a different origin and work on different scale lengths. In ball milling, the exfoliation is due to compression or shear forces caused by the movements of the balls, that in our case have a macroscopic diameter (3 mm). In sonication, the mechanical action arises from cavitation

bubbles, with radius of about one hundred of μm , that generate high strain rates in the surrounding liquid upon implosion.¹⁻³

Fig. 7 in main text shows the typical effects of treatment by sonication (Fig. 7b,c) and milling (Fig. 7d,e) on BN.

Sonication reduces the size of mesoscopic flakes, but does not change significantly their morphology. We previously studied the effect of sonication on materials by monitoring the evolution of surface roughness on bulk graphite sonicated in a solvent commonly used for graphene production, *N,N'*-dimethylformamide;³ in these conditions exfoliation proceeds on a layer-by-layer basis; only the upper part of the graphite is interested, and the process is slow, requiring several hours to have visible effects on the substrate roughness.

In case of milling, instead, the effects of shear and compression action of the milling spheres is visible on several flakes, with BN stacks shifted over each other, showing folds not only on the surface of the platelets (Fig. 7d, white arrows) due to the shear force of balls rolling over the top surface of the particle, but also *inside* the platelets, (Fig. 7e, white arrows) due to the compression force of milling balls colliding with the edge of the particle and then sliding over it, in agreement with the results obtained in ref.⁴

Both milling and sonication yield a large number of BN sheets after spin coating on silicon oxide substrates. The amount of exfoliated material estimated by AFM is found to be roughly proportional to BN concentration in solution. By assuming for BN an extinction coefficient $\alpha=2367 \text{ ml/mg/m}$ measured at 300 nm,⁵ an estimated concentrations up to 0.04 mg/ml, comparable to 0.06 mg/ml obtained by extensive sonication could be estimated; however, the presence of significant light scattering due to the large size of the sheets does not allow to use optical absorption data to estimate exfoliation yield. The absorbance *A* of all solutions showed a

power-law dependence of A on light wavelength λ ($A \propto \lambda^{-n}$), indicative of strong light scattering, in agreement with what observed in ref. ⁵.

The sheet morphology, as measured by AFM, is the one expected for layered materials, with linear edges and sharp corners (Fig. 2d), but the sheets have a wide distribution in lateral size (from tens of nm to more than 1 μm) and thickness (up to 10 nm, with no large macroscopic aggregates). It is thus difficult to discriminate any difference just by visual comparison of the AFM images.

Image analysis procedure

To characterize and define effectively nano-materials is a major metrological problem; as example, the exfoliation of the same starting solution shall give different yields of solubilized material and monolayers fraction if centrifuged at different speeds,⁶ or purified using different washing procedures.^{7,8}

It is fundamental to quantify not only the average size of the sheets obtained, but their size distribution as well; in this, 2D materials have some analogy with what is done routinely to characterize poly-dispersed, 1D polymers.⁹

For this, statistical analysis is needed to characterize the poly-dispersed sheets. This is commonly done through one-by-one localization and analysis of exfoliated sheets with Transmission Electron Microscopy (TEM). This approach, besides bring tedious and cumbersome, is also not fully objective, because smaller sheets shall escape from the TEM grid thus over-estimating the mean sizes of the exfoliated flakes and making the related statistics inaccurate. For example, the measurement uncertainty depends on the square root of the number of the detected sheets in case

of ensembles following Poisson statistics. Thus, a sample population of 100 measured sheets is associated with 10% of intrinsic error. The operator as well shall sometime focus on examining the most interesting (i.e. thinner) sheets while missing larger aggregates. Furthermore, sheets aggregation, restacking and folding on the TEM grid during solvent evaporation makes the analysis of size and shape of the sheets difficult. The number of sheets localized and measured by TEM can be very low, even below ten for a given nanosheet type, and even partially folded or overlapping sheets should be measured to improve the statistics.¹⁰

Thus, it is fundamental to complement published results obtained by TEM with more detailed studies, performed at the nanoscale and on large statistical data (see also section dedicated to Dynamic Light Scattering in the following text).

Atomic Force Microscopy (AFM) can be used to characterize the size distribution of thousands of nano-sheets, to automatically detect and analyze the length, area and surface density of them, and to compare the obtained results with more macroscopic characterization techniques such as optical spectroscopy and dynamic light scattering.

To quantify the sheet size obtained with different techniques, we used an image analysis software able to detect automatically individual sheets and measure their area and lateral size¹¹. In this way we could also remove noise and grains crossing the image edge, and plot the statistical distribution of the different observables measured. While AFM can easily give high-resolution images of the flakes and allow manual measurements of their size, several steps are required to obtain quantitative results on a statistical base.

a) Use of a flat substrate allowing a fast and unambiguous discrimination of the flakes from the surrounding bare substrate. This primary condition was satisfied by spin coating BN on atomic flat silicon substrate because the height of the single sheet (about 1 nm thick as measured by

AFM) is significantly larger than the root mean square roughness (RMS) of the substrate which amounts to 1.8 Å.¹²

b) Use of the correct flattening procedure to remove the AFM artefacts due to sample tilt, always present, and non-linearity of the piezoelectric scanner.^{13,14} Dedicated flattening procedures based on local mean or local standard deviation (SD) of the height values shall be used in case of irregular surfaces.¹¹ The first method simply subtracts the mean value of the pixels in the local neighbourhood of each pixel. The SD equalization scales the height values by a factor given by the standard deviation of the global image, divided by the local mean of the standard deviation. The efficiency and the reliability of the flattening procedure were monitored step-by-step by histogram analysis, plotting the frequency distribution in z of all the pixels of each image. In case of relatively flat substrates, the better is the flattening, the narrower is the measured height histogram, with a peak-width close to silicon roughness. The used procedure removes the artifacts in few steps and the measured substrate roughness rapidly converges in the range of values between 0.15 and 0.20 nm, in good agreement with the values reported in literature.

c) Once the image is flattened, a suitable height threshold is used to discriminate flakes from background. A binary condition selection is used: only the pixels above the threshold are considered belonging to a flake, while the rest is disregarded. Anything having a height lower than the threshold will be counted as background, and not included in the statistics. We choose 0.5 nm as a suitable threshold, a value half the thickness of a typical sheet and more than two times larger than the substrate RMS roughness.

d) A further filter shall also be applied. The filter will simply exchange small "ridge pixels" with interpolated values if the slope on the ridge is smaller than the given percentage of the maximum slope. We define a ridge pixel as a pixel having a value that is either larger or smaller than its

four next-neighbour pixels. In contrast to other filters, this filter will only affect the smaller corrugations. To eliminate larger noise peaks a Local Mean filter could be applied (see above).

e) Recognise connected or partially overlapping flakes by finding local minima, even above the threshold, that will be considered as flake edges.

Even if the software performs automatically all these operations, the parameters used for each operation (threshold height, noise filter, etc.) should be carefully tuned and cross-checked for reproducibility and reliability. However, the automatic detection of flakes is pretty robust and not so sensible to fine-tuning of these parameters, given that the flakes are usually deposited on very flat silicon substrates and that the lateral resolution of AFM is much larger than the average sheet size. In particular, we have found that the method is very suitable to analyze structures having a lateral size of tens of nanometers and uniform thickness, such as flakes of graphene, BN or other 2D materials. More details on the flake detection procedure shall be found in ref. ¹¹.

The first output of the AFM statistical analysis is simply the amount of sheets obtained for each process and treatment time, expressed in terms of number of sheets per square micron plotted in Fig. S6. Insets in Fig. S6 show the typical AFM images obtained at initial and final stages of the exfoliation, where the image analysis software has automatically identified and assigned a different colour to each BN sheet.

Of course, the most interesting output of the analysis is not the simple number of sheets, but their lengths and area (or size) distribution that was already discussed in main text.

We tried to use statistical histogram analysis to measure as well the AFM thickness of the sheets, as previously done with organic self-assembled monolayers ¹⁵ and with mono-atomic graphene oxide sheets. ¹⁶ However, the height histograms obtained did not yield well-defined peaks corresponding to the different BN layers, due to the strong dependence of this measurement on

the roughness of the sheets, which often show the presence of partial folds and nano-debris. Thus, the thickness was measured manually by profile analysis of different AFM scans, showing a skewed distribution similar to the ones observed for length (fig. S1). The thickness shows as well a decreasing trend (Fig. S7) similar to what observed for lateral size, with most of the material present as multi-layered sheets, and with all the samples distribution approaching an asymptotic average thickness of ≈ 6 nm; the values of average final thicknesses measured by AFM were: 8 ± 4 nm (High P. sonication), 6 ± 3 nm (Low P. sonication), 6 ± 3 nm (high P. Milling), 6 ± 3 nm (low P. milling). As mentioned in main text, we should keep in mind that these average values will not correspond to the median or to the highest peak of the size distribution $N(s)$, because they are not Gaussian.

Comparison of sheet size on surfaces and in solution

Statistically efficient techniques, able to estimate particle size quantitatively on large scale and in solution are light scattering techniques,¹⁷ such as dynamic light scattering (DLS) that has already been used to quantify the size and shape of graphene or graphene oxide (GO) sheets in solutions.^{18,19} A recent work has demonstrated that there is an empirical relationship between the sheet size measured by TEM and by DLS that, even if having relative errors up to 40%, shall be used to give a quick estimate of the average size of solubilized sheets.¹⁰ DLS measurements are affected by two key properties: solvation and sample shape. While the first kind of overestimation can be simply neglected for mesoscopic objects, the second point is not trivial. The DLS measurement is based on the assumption that all particles undergo Brownian motion in the solution and diffuse in the liquid like spherical particles; instead, 2D anisotropic sheets have

different diffusion coefficients, and thus one could not assume *a priori* that DLS will give the right measurement.^{18,19}

For a perfect sphere, Brownian motion is the same in all directions; for a linear nanostructure (like a nanotube), Brownian mobility is larger along the optical axis. For 2D sheets the large optical anisotropy shall align the flake orthogonal to the light polarization, with increased fluctuations in both longitudinal and transverse directions due to a higher contribution from rotational motion with respect to nanotubes, as demonstrated for graphene by Ferrari and co-workers.²⁰

The size evolution observed by AFM was thus compared with measurements performed in solution by DLS. The correspondence between the two techniques shall never be straightforward: AFM measures the sheets one by one, with high resolution, on a solid surface whereas DLS measures thousands of sheets at once, while floating in solution.

Fig. S3 and Fig. S5 compare the BN sheet size as measured by AFM and DLS. We see that both AFM and DLS techniques give a similar trend in size evolution, but with an offset between the measured s . A recent work by Coleman and coworkers¹⁰ reports for 2D materials an empirical power law correlation between the graphene nanosheets length, measured by TEM, and the first peak of the particle size distribution $a_{DLS} \propto L^{2/3}$. In our case, this empirical finding does not apply because we were interested in the original size distribution and did not perform any sorting of nanosheets size by centrifugation. Finding the right correlation between DLS signal and the “true” size of flexible, monoatomic, 2-Dimensional objects in solution will require much more experimental and theoretical work, and is out of the scopes of this paper. All we shall safely say is that, averaging on all samples, DLS gives an estimated size that is larger than the AFM measured one of ca. 20%. The 20% difference we observed between the size of a 2D sheet

measured on surface and in solution can be due to the complex hydrodynamic radius, the folding and the unknown refractive index of these 2D sheets in solution, that does not allow to use the Mie theory commonly used in DLS to infer the particles' radius from the scattering spectrum.

Final remarks: which is the best nanosheet shape for composites?

Overall, the statistical comparison of the samples indicates that the four different techniques give comparable results, with a lateral sheet size between 116 and 136 nm (as measured by AFM) and an average thickness of 6 nm, with a lateral size/thickness aspect ratio ≈ 20 .

The relevant size that should be monitored depends on the final application of the material; in general, for composites applications, both length and width are relevant and should be optimized. In particular, in order to produce stronger composites, the load transfer must be maximized and this would correspond to have a length larger than a critical minimal value (along the applied load) of the flake $L_{\min} \approx \sqrt{thE/G}$, where h is the thickness of the interface between matrix and the few layer graphene flake, t is its total thickness, E is the Young modulus of graphene and G is the shear modulus of the interface²¹. In order to have all the graphene mass working in the composite this minimal length is also the optimal one. However, because of the random orientation of the sheets, load transfer will take place along all sides of the sheets, and thus the size distribution of both L and W should be taken into account; maximizing both length and width means maximizing the average area of the sheet, to give a very good interaction with the surrounding matrix.

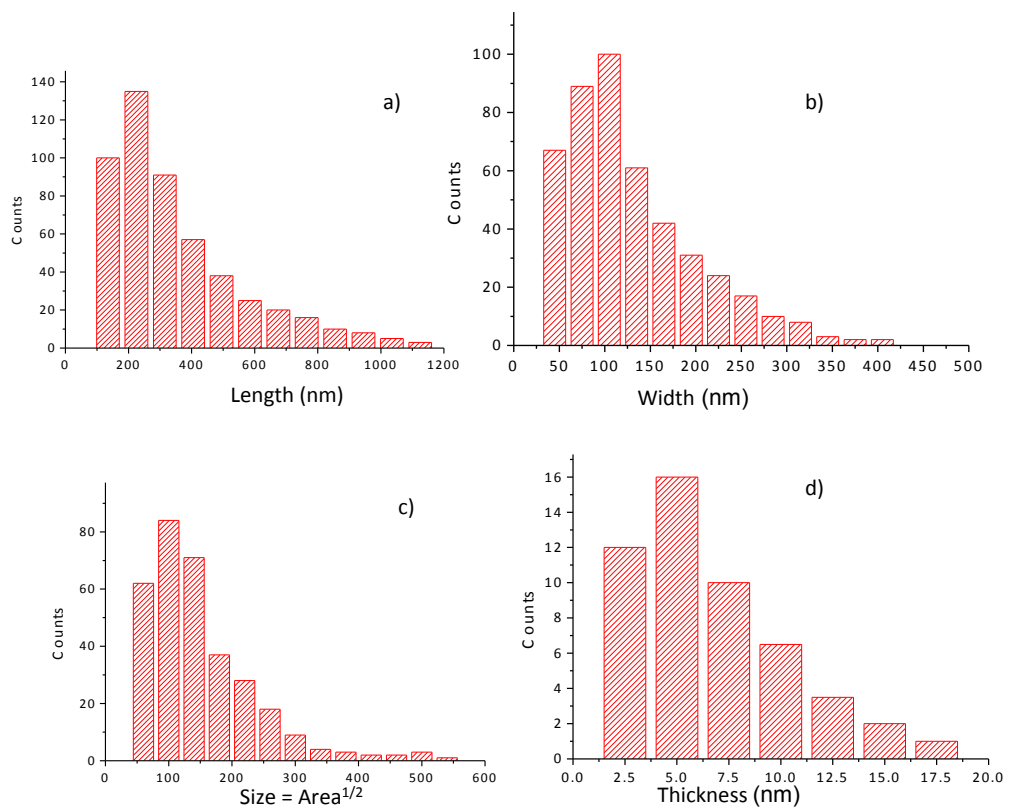


Fig. S1 Typical histogram distributions of various physical quantities of the nanosheets obtained by AFM image analysis, all featuring an highly skewed shape.

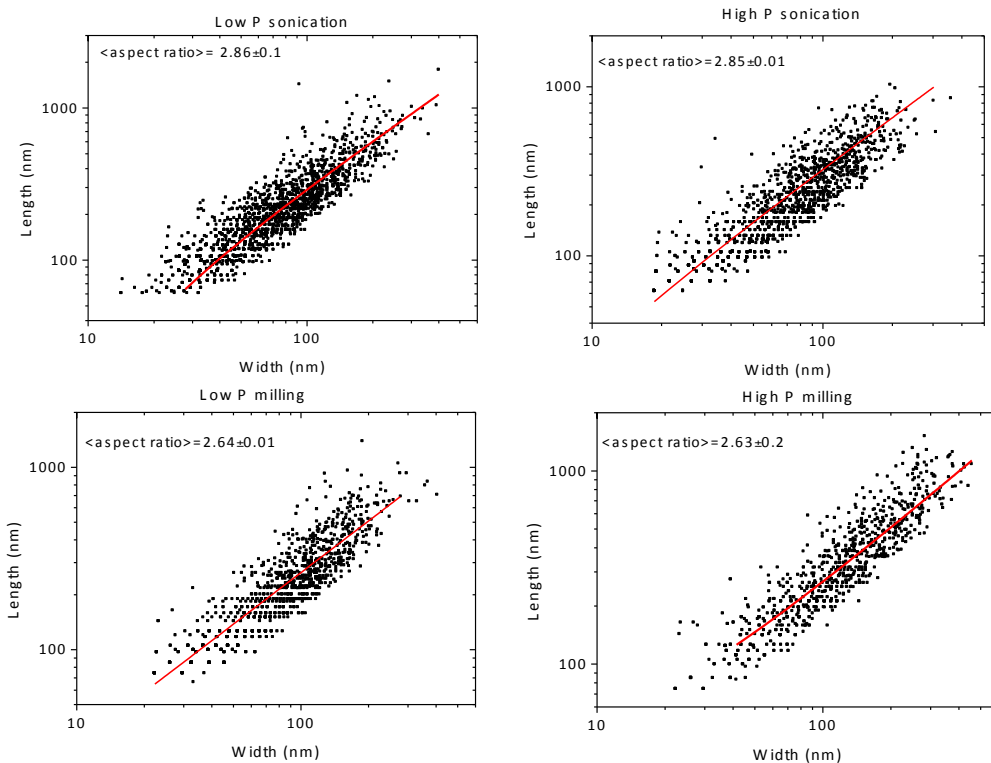


Fig.S2 Aspect ratio of length to width for all the BN samples exfoliated by milling and sonication, plotted in log-log scale. Red lines show the best linear fitting of the data points. The average slope is reported with its standard error in the inset of each graph.

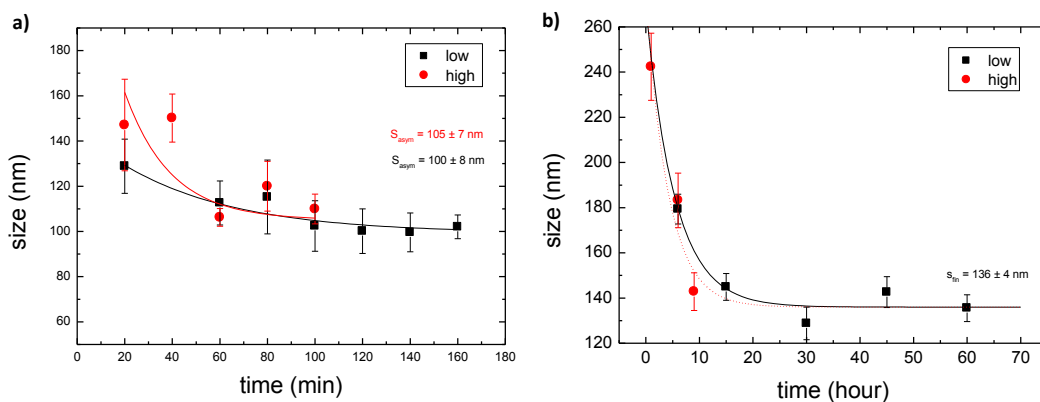


Fig. S3 Evolution of BN nanosheet size exfoliated by ultrasonication and Ball milling measured on a surface by AFM. All the data-set are fitted with exponential curves.

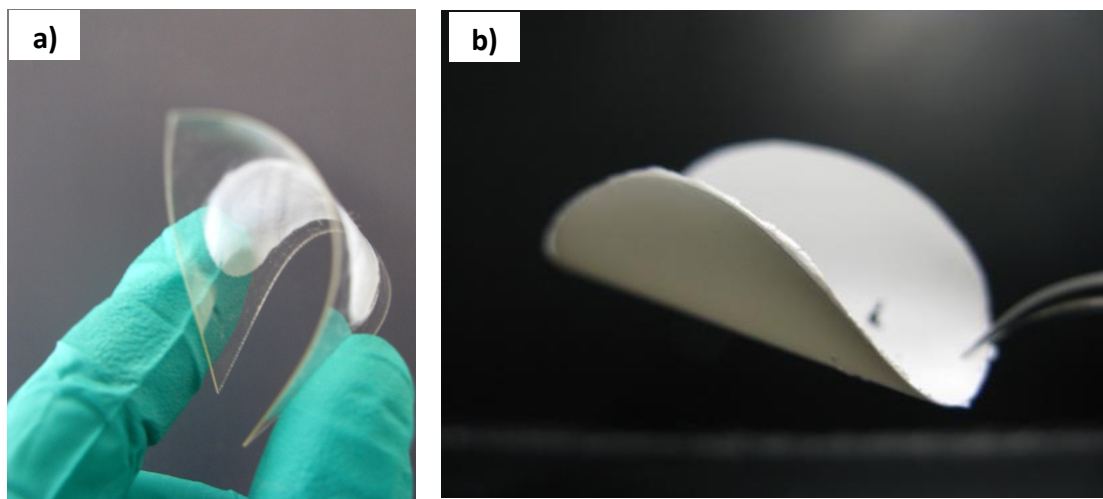


Fig. S4 a) BN membranes prepared from the BN solutions. a) thin layer deposited on PET. b) BN self-standing thick membrane.

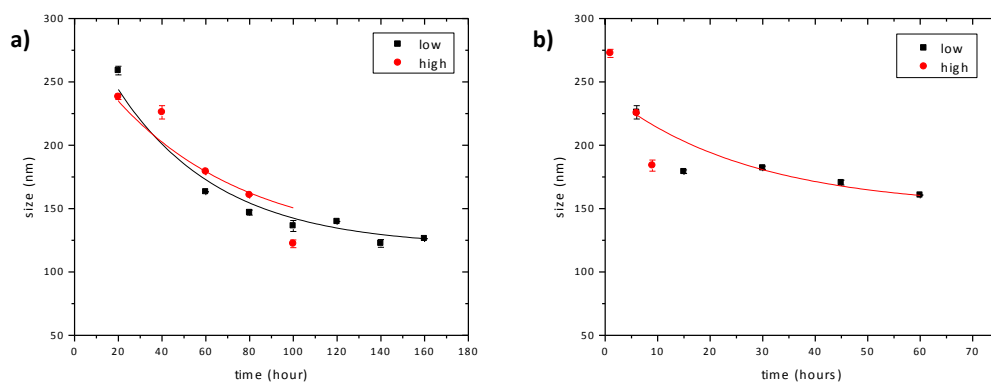


Fig. S5 Evolution of BN nanosheet size exfoliated by ultrasonication and Ball milling measured in solution by DLS. Lines show the corresponding exponential fit of the data.

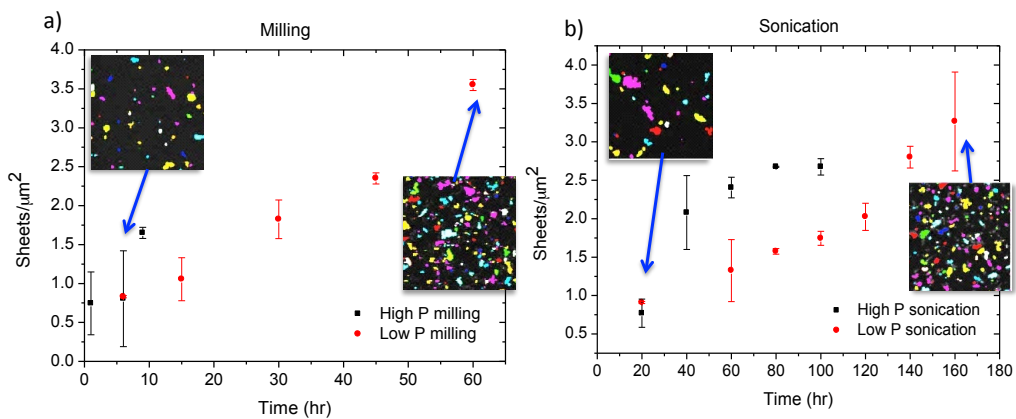


Fig. S6 Graphs representing the number of sheets counted per μm^2 for a) sonication and b) ball milling. Inside the graphs we also show typical processed images from the AFM analysis of the BN samples at lowest or highest concentrations.

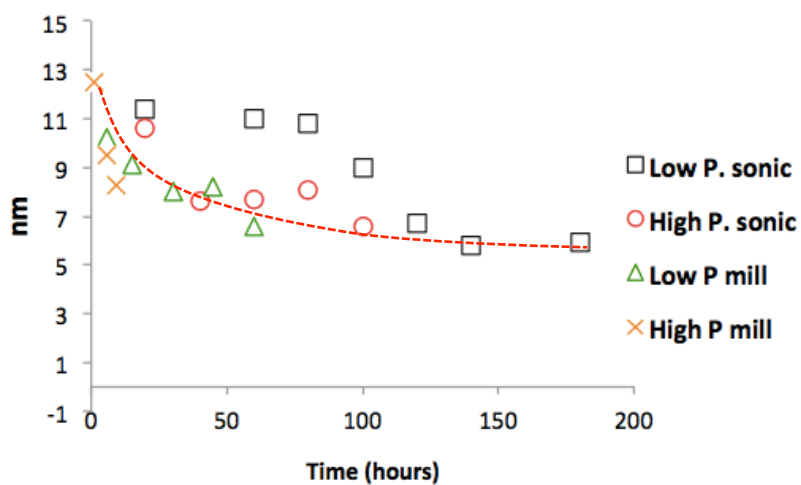


Fig. S7 Evolution of BN nanosheet thickness exfoliated by sonication and Ball milling in solution, measured by AFM. The lines are just a reference for the eye.

Table S1: Statistical distributions

	Equation $f(x)$	Reliability $N(x)$	Mean μ	Variance σ^2
Gaussian	$\frac{1}{w\sqrt{2\pi}} e^{-\frac{(x-x_0)^2}{2w^2}}$	$\frac{1}{2} - \frac{1}{2} \operatorname{erf}\left\{\frac{x-x_0}{w\sqrt{2}}\right\}$	x_0	w^2
Log-normal	$\frac{1}{xw\sqrt{2\pi}} e^{-\frac{(\ln x - x_0)^2}{2w^2}}$	$\frac{1}{2} - \frac{1}{2} \operatorname{erf}\left\{\frac{\ln x - x_0}{w\sqrt{2}}\right\}$	$e^{x_0 + w^2/2}$	$(e^{w^2} - 1)e^{2x_0 + w^2}$
Weibull	$\frac{k}{\lambda} \left(\frac{x}{\lambda}\right)^{k-1} \cdot e^{-(x/\lambda)^k}$	$e^{-(x/\lambda)^k}$	$\lambda \cdot \Gamma(1 + 1/k)$	$\lambda^2 \cdot \Gamma(1 + 2/k) - \mu^2$
Gamma	$\Gamma(\alpha) x^{\alpha-1} e^{-\beta x}$	$\frac{1}{\Gamma(\alpha)} \gamma(\alpha, \beta x)$	$\frac{\alpha}{\beta}$	$\frac{\alpha}{\beta^2}$

note:

$$\text{error function: } \operatorname{erf}\{z\} = \frac{2}{\sqrt{\pi}} \int_0^z e^{-t^2} dt$$

$$\text{lower incomplete } \Gamma \text{ function: } \gamma(\alpha, x) = \int_0^x t^{\alpha-1} e^{-t} dt$$

Table S2: Exfoliation techniques used (see text for more details)

Procedure	High Power	Low Power
Sonication	220 W (effective power)	66 W (effective power)
Ball milling	450 rpm (rotation speed)	200 rpm (rotation speed)

REFERENCES

- 1 Hennrich, F. *et al.* The mechanism of cavitation-induced scission of single-walled carbon nanotubes. *Journal of Physical Chemistry B* **111**, 1932-1937, (2007).
- 2 Khan, U. *et al.* Solvent-Exfoliated Graphene at Extremely High Concentration. *Langmuir* **27**, 9077-9082, (2011).
- 3 Xia, Z. Y. *et al.* The Exfoliation of Graphene in Liquids by Electrochemical, Chemical, and Sonication-Assisted Techniques: A Nanoscale Study. *Advanced Functional Materials*, DOI: 10.1002/adfm.201203686, (2013).
- 4 Li, L. H. *et al.* Large-scale mechanical peeling of boron nitride nanosheets by low-energy ball milling. *Journal of Materials Chemistry* **21**, 11862-11866, (2011).
- 5 Coleman, J. N. *et al.* Two-Dimensional Nanosheets Produced by Liquid Exfoliation of Layered Materials. *Science* **331**, 568-571, (2011).
- 6 Khan, U. *et al.* Size selection of dispersed, exfoliated graphene flakes by controlled centrifugation. *Carbon* **50**, 470-475, (2012).
- 7 Schlierf, A. *et al.* Nanoscale insight into the exfoliation mechanism of graphene with organic dyes: effect of charge, dipole and molecular structure. *Nanoscale* **5**, 4205-4216, (2013).
- 8 Yang, H. *et al.* A simple method for graphene production based on exfoliation of graphite in water using 1-pyrenesulfonic acid sodium salt. *Carbon* **53**, 357-365, (2013).
- 9 Palermo, V. Not a molecule, not a polymer, not a substrate... the many faces of graphene as a chemical platform. *Chemical Communications* **49**, 2848-2857, (2013).
- 10 Lotya, M., Rakovich, A., Donegan, J. F. & Coleman, J. N. Measuring the lateral size of liquid-exfoliated nanosheets with dynamic light scattering. *Nanotechnology* **24**, #265703, (2013).
- 11 (Scanning Probe Image Processor, version 2.0000, Image Metrology A/S, Lyngby, Denmark.).
- 12 Gentile, P. *et al.* STM study of ultra-thin (< 2 nm) silicon oxide. *Journal of Non-Crystalline Solids* **322**, 174-178, (2003).
- 13 Liscio, A. Scanning Probe Microscopy beyond Imaging: A General Tool for Quantitative Analysis. *ChemPhysChem* **14**, 1283-1292, (2013).
- 14 Morita, M., Ohmi, T., Hasegawa, E., Kawakami, M. & Ohwada, M. GROWTH OF NATIVE OXIDE ON A SILICON SURFACE. *Journal of Applied Physics* **68**, 1272-1281, (1990).
- 15 Palermo, V. *et al.* Scanning probe microscopy investigation of self-organized perylenetetracarboxydiimide nanostructures at surfaces: Structural and electronic properties. *Small* **3**, 161-167, (2007).
- 16 Liscio, A. *et al.* Charge transport in graphene-polythiophene blends as studied by Kelvin Probe Force Microscopy and transistor characterization. *Journal of Materials Chemistry* **21**, 2924-2931, (2011).
- 17 Los, S. *et al.* Cleavage and size reduction of graphite crystal using ultrasound radiation. *Carbon* **55**, 53-61, (2013).
- 18 Catheline, A. *et al.* Solutions of fully exfoliated individual graphene flakes in low boiling point solvents. *Soft Matter* **8**, 7882-7887, (2012).
- 19 Shih, C. J., Lin, S. C., Sharma, R., Strano, M. S. & Blankschtein, D. Understanding the pH-Dependent Behavior of Graphene Oxide Aqueous Solutions: A Comparative Experimental and Molecular Dynamics Simulation Study. *Langmuir* **28**, 235-241, (2012).
- 20 Marago, O. M. *et al.* Brownian Motion of Graphene. *Acs Nano* **4**, 7515-7523, (2010).
- 21 Pugno, N. M. The design of self-collapsed super-strong nanotube bundles. *Journal of the Mechanics and Physics of Solids* **58**, 1397-1410, (2010).